Crystal structure of the low temperature phase (II) of polytetrafluoroethylene

J. J. Weeks, E. S. Clark* and R. K. Eby
National Bureau of Standards, Polymer Science and Standards Division, Washington, D.C. 20234, USA
(*Received* 8 *May* 1981)

An electron diffraction pattern from polytetrafluoroethylene in Phase II was analysed to determine a chain conformation of 2.1598 CF_2 units per turn of the helix. A structure was established from a combination of electron and X-ray diffraction data. The structure contains an ordered repeating pattern of a left- right-handed pair of chain stems. Although the structure is ordered in three dimensions, it cannot be described meaningfully in terms of classical space group nomenclature because very small changes in the structure result in very large changes in the cell parameters. The structure has a volume of 0.03542 nm^3 per CF_2 group, corresponding to a density of 2344 kg m^{-3}.

INTRODUCTION

Polytetrafluoroethylene, PTFE, exhibits a well-ordered phase II crystal structure below its solid–solid transition at 292K. Bunn and Howells[1] assigned to the chains a helical conformation with 13 carbon atoms making six turns in a chain repeat distance of 1.68 nm. They found that the chain stems are packed on a nearly hexagonal array with the cell dimensions, projected on the (001) plane, being $a' = b' = 0.554$ nm and $\gamma' = 119.5°$. Clark and Muus[2] refined these values to 0.559 nm and 119.3° at 273K with $c = 1.688$ nm. As a result of measuring the layer spacings in electron diffraction patterns from PTFE fibres, Clark *et al.*[3,4] found that the assumed commensurable 13/6 helix is not exact, but rather is untwisted slightly. Initially it was assumed that the unit cell of the low temperature phase contained only one chain, but more recently a number of authors[5–7], on the basis of spectroscopic measurements, have proposed that the cell must contain two chain stems. With the exception of a triclinic cell derived by Kilian[8] from X-ray powder diffraction, no complete set of three-dimensional cell parameters has been given for PTFE.

The electron diffraction fibre patterns show a remarkably large number of well-resolved reflections for a synthetic polymer, as may be seen in *Figures 1–3*. By careful measurement of these patterns, we found that the unit cell proposed by Kilian was not applicable to our phase II PTFE sample. As will be seen, several triclinic packing modes were found which can account for our diffraction pattern. One of these modes was used for preliminary calculations which compared the calculated X-ray scattering intensity distribution for a powder with the one we obtained from a sintered PTFE sample.

SAMPLE AND METHOD

The electron diffraction work was done in 1957 at the Du Pont Experimental Station on unsintered PTFE moulding powder of 90–100% crystallinity. The preparation of the highly-oriented fibres from fractured compressed pellets has been described earlier[3,4]. An electron diffraction (only) unit operating at 45 kV was used to produce the patterns. Sample to film plate distance was ~500 mm. Numerous samples and various exposure times were tried in order to obtain the symmetrical fibre patterns shown in *Figures 1–3*. Transformation of the PTFE fibres from the room temperature phase (IV) to the low temperature phase (II) was accomplished by storing them on dry ice for several hours. No control of the sample temperature in the diffraction unit was possible, but it is assumed that the pattern can be calibrated by adjustment of the electron wavelength to normalize the 0-layer reflections to the X-ray diffraction value[2] ($a' = 0.559$ nm). The three patterns shown were measured on a two-dimensional direct-reading comparator having 1 μm resolution. Most of the layer lines were also traced on a recording microdensitometer with 10:1 linear magnification.

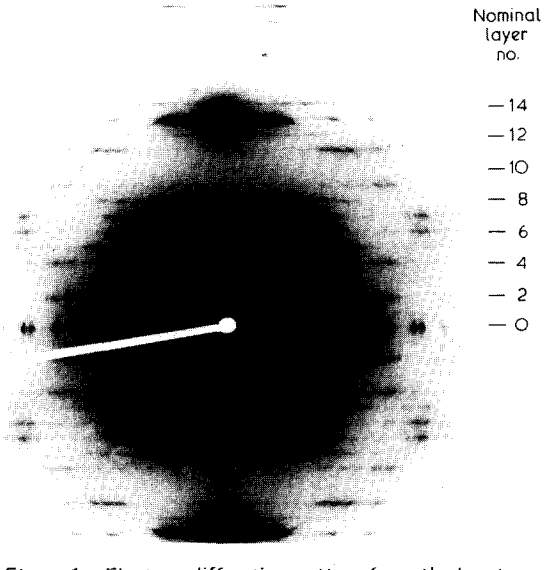

Figure 1 Electron diffraction pattern from the low temperature phase of polytetrafluoroethylene; plate A. The fibre axis is vertical

* Permanent address: Polymer Engineering, University of Tennessee, Knoxville, TN 37916, USA

0032-3861/81/111480-07$02.00

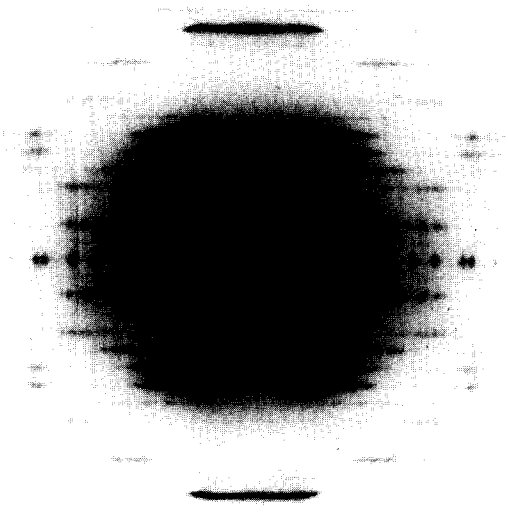

Figure 2 Electron diffraction pattern from the low temperature phase of polytetrafluoroethylene; plate B

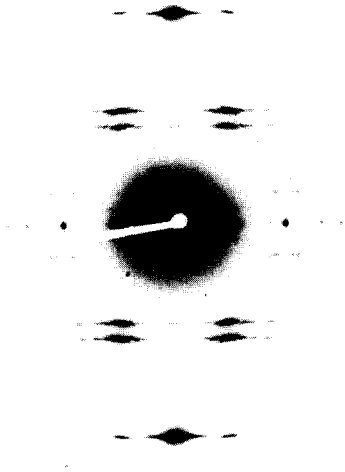

Figure 3 Electron diffraction pattern from the low temperature phase of polytetrafluoroethylene; plate C

In order to obtain reliable intensity data on PTFE, an X-ray powder diffractometer was used to scan a highly crystalline sintered and annealed sheet of the polymer at temperatures of 259 and 275K. This sample is the same material mentioned in ref 9, where it was designated no. 20 and was found to be 78% crystalline. A scan of the same sample in phase IV (at 296K) was used as a guide in drawing a continuous background under the low temperature phase diffraction peaks. Copper radiation ($\lambda = 0.154183$ nm) was used with a carbon monochromator before the scintillation detector; the scanning speed was 1/4 degree 2θ per min.

As described later, the unit cell parameters serve only as a computational aid and do not describe the structure meaningfully. However, in order to calculate diffraction intensities, it was necessary to postulate a 'computational unit cell' that could be used in the structure factor formula. The method applied to derive the computational unit cell corresponding to a specific packing mode consists of a comparison between the observed electron diffraction 2θ values (corresponding to copper radiation) with the set calculated from the computational cell being considered. We have used the average squared 2θ difference between observed and calculated diffraction angles as a measure of the 'goodness of fit' of a trial cell. This value will be designated by the letter 'G'. Since the fibre axis is along c and since a^*, b^*, and γ^* are known if the number of chains in the unit cell is known, the complete cell is determined by finding two additional parameters. These can conveniently be the x and y components of c^* in a Cartesian coordinate system having b^* along the y-axis and c along the z-axis[10]. Let us label these required values X and Y and express them in λ/d (i.e., dimensionless) units. Because the nominal[4] first layer 2θ values are the least sensitive to X and Y, a fairly coarse grid can be used to search for the possible computational cells. Calculation showed that for the one-chain cells, an x,y-grid size of 0.005 by 0.005 is sufficiently fine for mapping in that no reflection would change its 2θ value by more than 0.3° in going from one grid point to the next. Once a local grid minimum was found for G, a search on successively finer grids was used to establish a 'best-fitting' trial cell. The cells which give reasonable agreement with the 2θ values observed on the nominal first layer can then be used as trial cells for comparison with 2θ values from the higher layers.

Initially we tried to account for the non-uniform layer spacing by using the observed apparent c value of each layer. Alternatively, a non-integral l index could be used. However, as will be seen below, this initial approach did not lead to a satisfactory cell.

ELECTRON DIFFRACTION DATA

Table 1 gives the 2θ data derived from the 0-layer measurement of diffraction plate A, shown in *Figure 1*. Calibration of the electron wavelength using $a' = b' = 0.559$ and $\gamma' = 119.3°$ gave $\lambda = 5.715$ pm and a standard deviation from the calculated 2θ values of 0.06°. The 2θ value of a non-zero layer reflection was derived from the average radius of the four corresponding spots after taking their average position as a centre. Examination of the relative displacement of corresponding spots on the upper and lower nominal 13th layers allowed a determination of any tilt of the fibre specimen and subsequent correction of the layer heights. Because plate A showed the least fibre tilt and exhibited the largest number of measurable spots, it was used for the analysis to follow. *Table 2* shows those 2θ values from the non-zero

Table 1 Diffraction angles, 2θ (copper), from the 0-layer of plate A

Observed (deg)	Calculated (deg)	Observed (deg)	Calculated (deg)
18.23	18.26*	66.97	66.96
31.69	31.68	69.33	69.33
36.73	36.88	69.78	69.79
37.24	37.28	70.24	70.30
49.26	49.31	78.47	78.48
49.88	49.83*	79.49	79.47
56.58	56.64	87.96	87.90*
57.34	57.30	92.80	92.92*
66.08	66.17	94.16	94.11

* Weighted average of two reflections

Table 2 Observed 2θ-values for 'computational cell' refinement from diffraction plate A

Layer no. if helix is: 13/6	54/25	473/219	2θ-angle* (deg)
1	4	35	20.86, 22.72, 25.39, 28.85, 30.99, 33.18, 35.50, 37.33
2	8	70	26.94, 30.43, 33.91, 34.81, 40.07, 41.08, 42.80, 45.04, 49.28, 52.30, 54.04, 58.46, 59.59, 61.60
5	21	184	29.96, 30.84, 33.84, 36.84, 38.98, 41.06, 42.06, 43.56, 44.90
6	25	219	31.94, 32.91, 33.76, 36.91, 39.54, 41.49
7	29	254	37.22, 38.63, 39.72, 43.54, 45.32, 48.75

* Wavelength = 0.154183 nm. The values are the average of three replicate measurements and the variance is 0.00305 with 86 degrees of freedom

layers which were used in refining the possible cells. We begin by considering cells containing only one chain stem.

COMPUTATIONAL CELL RESULTS

One chain cells

A search in reciprocal space for X and Y values leading to a good fit of the combined 2θ set for nominal layers 1 and 2 was possible because the apparent c values for these two layers agreed within 0.1%[4]. From geometry, it is generally necessary to map one-half the a^*b^* area to find a possible cell. In the case of PTFE, the one-chain cells have $a^* = b^*$, so that only one-fourth the area need be searched. The initial mapping showed three regions where G was less than 0.3 deg^2. By searching to the local minima, G values of 0.211, 0.213, and 0.262 deg^2 were obtained for the best-fitting cells. The best of these cells had 17 reflections which fit within 0.3°, but there were 5 differences greater than 0.3°, the largest being 1.3°. It is clear that a single triclinic cell containing only one chain stem cannot account for our observed diffraction pattern.

Two-chain cells

When the cell volume is doubled by adding a second chain stem to the computational cell, the results of the derivative lattice theory[11] must be used to find the projected cells to be considered. The general theory gives 7 possible cells, but since c in our case remains fixed and $a' = b'$, only two choices arise: (A) $a'' = 2a' = 1.118$ nm, $b'' = b' = 0.559$ nm and $\gamma'' = 119.3°$ and (B) $a'' = 2a' = 1.118$ nm, $b'' = 0.5649$ nm and $\gamma'' = 59.65°$.

(1) Type (A) cells

On account of the smaller size of a^*, due to the doubling of a', it is necessary to reduce the grid size in the x-direction by a factor of two in order to maintain a tolerance of 0.3° for 2θ changes. In this case, half the a^*b^* area must be mapped, and again we used the combined nominal 1st and 2nd layer 2θ values listed in *Table 2*. Five possible cells were found having G values less than 0.05 deg^2; the best one being 0.024 deg^2. For this cell only one 2θ difference exceeded 0.3°; however, this difference of 0.60° seemed to be too great for the fairly strong 1st layer reflection at 25.39°. Since we believe the data on the zero-, first-, and second-layers are self-consistent within 0.3° error, it appears there is no two-chain type (A) cell which is consistent with our diffraction pattern.

(2) Type (B) cells

A projected cell equivalent to type (B) was used for the initial mapping of this lattice. This cell has $a'' = 0.96478$ nm, $b'' = 0.56490$ nm, and $\gamma'' = 90.00°$. It will be convenient to consider one chain axis to be at the origin and one to be in the centre of the cell. Since $\gamma^* = 90°$, only one-fourth the a^*b^* area need be searched; a 0.0025 by 0.005 grid was used. Only one region was found where G was less than 0.05 deg^2, and upon searching to the local minimum, a G value of 0.0015 deg^2 was achieved. This corresponds to a standard deviation of 0.04°, a value better than that from the 0-layer fitting. The X,Y values for this best trial two-chain cell were $X_1 = 0.039343$, $Y_1 = 0.056224$. Three other equally good cells can be derived from (X_1,Y_1); their c^* components are $(a^*\text{-}X_1,Y_1)$, $(X_1,b^*\text{-}Y_1)$ and $(a^*\text{-}X_1,b^*\text{-}Y_1)$. Designate these four cells as P_1 through P_4. If we now consider the remaining values of 2θ listed in *Table 2* and search the P_1 to P_4 cells to a minimum G value, we obtain poor agreement between observed and calculated 2θ values on the upper layers (G varies from 0.039 to 0.059), even though a correction is made for the varying apparent c dimension. A different approach was needed to account properly for the unequal spacing of the layer lines in PTFE. It was necessary to devise a commensurable approximation for the helix which may well be incommensurate. Previously[4] we have shown that a 54/25 = 2.1600 helix gives a better approximation of the units/turn ratio for our fibre sample than does a 13/6 = 2.1666 helix. This former helix was derived under the assumption that the spacing of the repeating CF_2 unit (~0.130 nm) for a 13/6 helix would be the same as that measured for the helix in our sample. It is not, however, necessary to make this assumption, as the following section shows.

Helix repeat period

As previously noted, the layer spacings on the diffraction plates are not uniform[4]. Since each observable layer in PTFE has its intensity controlled by a single low-order Bessel function, an incommensurable helix will cause an entire layer to be displaced from the position predicted by any approximate commensurable helix, such as the 13/6 helix. The amount of the displacement can be derived from the condition for diffraction from a discontinuous helix[12]:

$$\zeta = n/P + m/s \qquad (1)$$

where ζ is the layer height from the reciprocal lattice origin, n is the integral order of the Bessel function, P is the pitch of the helix, s the projected distance (on the axis) between like units, and m any integer. For any commensurable helix, the repeat period, $c_0 = t \cdot P = u \cdot s$, where t is the integral number of turns in the integral number of units, u. Some such commensurable helix always can be found which gives the actual units per turn ratio to a sufficient approximation. We derive the u/t helix by successive calculations beginning with the observed spacings of layer lines having index l:

$$\zeta_l = l/c_0 = n/P + m/s \qquad (2)$$

Thus:

$$l\,dc_0/c_0^2 = n\,dP/P^2 + m\,ds/s^2 \quad (3)$$

since c_0 will be changed if P and/or s are changed slightly, but the apparent layer number will not change until a new helix is derived. Starting with the observed apparent repeat period, $\tilde{c}$, from each layer and the approximately correct 13/6 helix ($t=6$, $u=13$), we obtain least squares estimates of c_0, ΔP and Δs by applying the following equation to each layer simultaneously.

$$\Delta c \equiv \tilde{c} - c_0 \simeq nt^2\Delta P/l + mu^2\Delta s/l \quad (4)$$

The initial values for P and s can be obtained from c_0 and thus new values can be found.

$$P = c_0/t + \Delta P \quad (5)$$

$$s = c_0/u + \Delta s \quad (6)$$

Next a new commensurable helix is derived by finding some integral number of turns (arbitrarily restricted to less than 500) which will make $u\,(=Pt/s)$ an integer within a tolerance of 0.01. The helix with the smallest error is chosen. The layers can then be reindexed by using the relation, $l=tn+um$, and new apparent c's can be calculated for each observed layer from l/ζ_l. Note that n (and m) values do not change for the new helix, since only layer lines of low order n have observable intensities[12].

One iteration of this process gave a satisfactory commensurable helix for plate A; $c_0 = 61.486 \pm 0.035$ nm, $u=473$, $t=219$, and $u/t=2.1598$. For plate B, shown in *Figure 2*, we derived a somewhat different helix, 147/68 $=2.1618$, with $c_0 = 19.061 \pm 0.007$ nm. If the P_1 cell is used with both of these c values to calculate 2θ sets, we find quite similar values on the '1st' layer, agreeing to within 0.1°, but on the higher layers the dissimilarities become more pronounced. It is not unlikely that differences in temperature and sample conditions may affect the pitch of the helix. It was decided to continue the calculations using both the 54/25 helix found previously[4] for plate A ($c_0 = 7.016 \pm 0.005$ nm) and the more accurate 473/219 helix. As shown in *Table 2*, the first observable layer ($n=-2$) has $l=4$ for the former helix and $l=35$ for the latter one. It should be noted that there are other commensurable helices with very similar pitch and spacing which should also give a good fit to the data but which were not evaluated.

Translationally equivalent cells

(1) The 54/25 helix

In the case of a 54/25 helix, cells P_1 to P_4, which account very well for the nominal 1st layer 2θ values, actually arise from a fit of data for which $l=4$ instead of $l=1$. This being the case, there are (by translational equivalence) 16 times as many possible triclinic cells which will have equally good G values on the nominal first and second layers*. These other cells can be found by translation of the points defining cells P_1 to P_4 by four axial repeats in each direction. The equations are:

$$X = (X_j(P_i) + ua^*)/j \qquad (u=0,1,2,3) \quad (7a)$$

$$Y = (Y_j(P_i) + wb^*)/j \qquad (w=0,1,2,3) \quad (7b)$$

For this case, $j=4$ and $i=1$ to 4. Half of these cells are always redundant by virtue of the inversion centre at the origin of reciprocal space.

Once the translationally equivalent cells are found, the complete set of observed 2θ values (given in *Table 2*) can be compared with a calculated set to compute a G value. The best fit of a 54/25 helix cell after refinement was obtained with $X=0.05035$ and $Y=0.05504$ for which $G=0.019$. Only one 2θ difference exceeded 0.3°; that being a discrepancy of 0.32° for the $l=8$ peak at 40.07°. Assuming that an estimate of the precision of the 2θ values can be made by examining the variation of repeated measurements, the adequacy of the cell can be assessed by means of an F test. Such a test was made on the G value by comparing it to the variance from replicate measurements of plate A (ratio = 6.5 with 41 and 86 degrees of freedom). There is almost no probability of such a large G value by chance alone. This result indicates that the 54/25 helix is not a sufficiently accurate approximation for the PTFE helix.

(2) The 473/219 helix

For the 473/219 helix, the initially calculated X and Y values for cells P_1 to P_4 are actually from the 35th layer. Thus j is 35 and v and w in equation (7) range from 0 to 34; however, 0 to 17 is sufficient to define all unique cells in our case because $\gamma^* = 90°$. The 1296 cells having a good fit on layers 35 and 70 can be reduced in number by three other restrictions in the observed diffraction pattern. It can be seen in *Figures 1–3* that there are near-meridional reflections on the nominal 6th, 7th, and 13th layers ($l=219$, 254, and 473), and that these are true diffraction spots, not simply a result of an increase in intensity from the transform of the helix. By measuring ξ (the cylindrical radius in reciprocal space) for each of these three reflections and defining twice the measured values as necessary conditions to be met by any proposed cell, we found 196 possible cells for the 473/219 helix. After G values had been calculated for these cells, using 2θ values from five layers, those having a value less than 0.1 were refined to a minimum.

After the refinement, there remained 5 cells with G values less than 0.0047 (the 95% confidence level). These cells are listed in *Table 3*. The G values for these cells are reduced by more than a factor of 4 from the best value for the 54/25 helix cells, with no increase in the number of reflections possibly having an observable intensity. The numerous layers on which the intensities are controlled by

Table 3 Possible two-chain 'computational cells' for PTFE from electron diffraction*

Cell no.	473/219 helix		Repeat units		G (deg^2)
	X	Y	Z_a	Z_b	
1	0.005728	0.068622	−16.9	−118.9	0.0040
2	0.005725	0.099790	−16.9	−172.9	0.0032
3	0.023957	0.099790	−70.9	−172.9	0.0038
4	0.042196	0.068622	−124.9	−118.9	0.0042
5	0.042202	0.099790	−124.9	−172.9	0.0036

* For each cell, $c = 61.486$ nm, $a^* = 0.15981$, $b^* = 0.27294$, and $\gamma^* = 90°$

* Both nominal layers 1 and 2 were used together in the X,Y search because they have the same apparent repeat period. This is derivable from equation (4) and was observed to be true on our diffraction plates

Table 4 *R* values found during structure refinement

R	*B* (nm²)	$\langle\Delta\phi^2\rangle$ (rad²)	$\langle\Delta Z^2\rangle$ (nm²)
0.272	0.05	0	0
0.246	0.05	0.035	0
0.217	0.05	0.035	0.0005
0.198	0.09	0.035	0.0005

high order Bessel functions can only give a weak background continuum such as is seen in *Figures 1* and *2*. The best fit cell was number 2 with $G=0.0032$ deg², a standard deviation of 0.06°. This is as good as the internal consistency of the 0-layer data. *Table 3* also lists the *z*-component, *Z*, of the *a* and *b* vectors, expressed in terms of repeat units along the helix. It is seen that all the cells have one of three values of Z_a and one of two values of Z_b, and further, that the respective values differ from one another by exactly 54 repeat units. (Note that in a 473/219 helix, repeat units differing by 54 can be made translationally equivalent by a rotation of the helix about its axis by approximately 0.76°.) Thus it appears that the different cells arise from rotation of an adjacent chain in the *a'*-direction by an angle in the range −44.90 to −46.42° with an accompanying translation of approximately 0.013 nm. Likewise, in the *b'*-direction, the rotation would be either 35.01 or 35.77° with a similar translation. (The signs of the angles are given for left-handed helices. For right-handed helices, the signs would be reversed.) From this viewpoint, we see that the various possible unit cells can arise from essentially a single structure. We subsequently emphasize the significance of this feature.

Calculations were made to determine whether cell no. 2, which best fits the electron diffraction data, would account for the intensity distribution observed by X-ray diffraction from a sintered PTFE powder. Other cells could be considered, but similar results are anticipated.

X-RAY INTENSITY CALCULATION

First, nine 2θ values from the 0-layer were refined to provide the estimates $a'=0.559098$ nm and $\gamma'=119.328°$ applicable to the particular sample used. Corrections to the 2θ angles were found by scanning a silicon standard under the same conditions, and the temperature shift to 273K was accomplished by interpolation of the two polymer scans. A set of 400 intensity values was taken from the scan in the range 28 to 48° at 0.05° increments. This region includes peaks from the nominal 0 through 8th layers and encompasses most of the diffraction intensity except for some of the 0-layer peaks and the strong peak from the nominal 13th layer at 72.78°. There are approximately 200 reflections in this range (including those falling within 0.5° of either end), and these were used as input to an intensity programme. In order to simplify the calculation, a uniform 54/25 helix was used with 473/219 helix cell parameters except for *c* which was reduced to 7.0270 nm (=61.486·4/35). Such a procedure also requires that non-integral *l* indices be used for layers above the 8th. Cylindrical atomic coordinates—(0.0406 nm, 0°, 0 nm) for carbon; (0.160 nm, −42°, 0.009 nm) for fluorine-1; (0.160 nm, 42°, −0.009 nm) for fluorine-2—were assigned to the initial CF_2 repeating group, and the helical chain was generated about the positive *z*-axis. Positive angular increments give a left-handed helix. The cell-centred helix was generated similarly and was either of the same hand or of opposite hand to the one at the origin. At the start, an isotropic temperature factor, *B*, of 0.05 nm² was assumed for all atoms.

After computation of the intensities for the trial structure, the X-ray diffraction scan was computed by assigning a modified Lorentzian[14] shape (width at half height = 0.25°) to individual reflections and summing the overlapping intensities. This calculated diffraction curve was then sampled at the cell diffraction angles and an *R*-value was computed from the calculated intensity, I^c, according to equation (8) by comparison with the interpolated observed intensity, I^0.

$$R \equiv \frac{\sum_i |KI_i^0 - I_i^c|}{K\sum_i I_i^0} \tag{8}$$

The scaling factor, *K*, was calculated to minimize the quantity $\sum_i((I_i^0)^{1/2}[KI_i^0 - I_i^c])^2$.

Initially, the structure refinement consisted of a rotation of the cell-centred helix about its axis and a translation along its axis, together with small changes in the *X* and *Y* values for the cell. Approximately 50% better *R* values were obtained when the two helices in the unit cell were of opposite hand instead of being of the same hand. Under this condition, cell no. 2 gave the *R* values which are listed in *Table 4* as the refinement progressed. In this table, $\langle\Delta\varphi^2\rangle$ and $\langle\Delta z^2\rangle$ are parameters for rotational and translational disorder as defined in ref 15. The values of the disordering parameters required to bring *R* below 20% seem large. However, this could be the result of the presence of several nearly identical structures, as well as rotational and longitudinal displacements of the helices in the sample. Energy calculations[16] for the 54/25 helix indicate that significant rotations and translations are possible as well as a number of nearly identical structures. Indeed, the other cells listed in *Table 3* yield *R* values similar to those in *Table 4*. In addition, the commensurable approximation for the helix was derived from oriented fibrils and may not be as good an estimate for the powder sample. It seems probable that other commensurable helices with very similar pitch and spacing would exhibit similar conformational energies and could be present. In any case, the results are sufficient to allow a structure to be given for phase II PTFE. This structure can be described by giving the rotations of adjacent chains about their axes and by their translations from a plane normal to the chain direction. *Figure 4* shows such a plane where the positions of the nearest carbon atoms are given. (The carbon radius is not drawn to scale.) The originally assumed atomic parameters: C–C distance of 1.53 Å; C–F distance of 1.33 Å; F–C–F– angle of 108° were not varied. A change in the tilt angle of the F–C–F– plane (85° from the chain direction) did not improve *R*. The cell *X* and *Y* values at minimum *R* were 0.0057296 and 0.099797, respectively. *Figure 5a* shows the computed diffraction pattern, which may be compared with the experimentally obtained scan in *Figure 5b*.

CONCLUSIONS

Several possible triclinic 'computational unit cells' were found for phase II PTFE from analysis of the electron

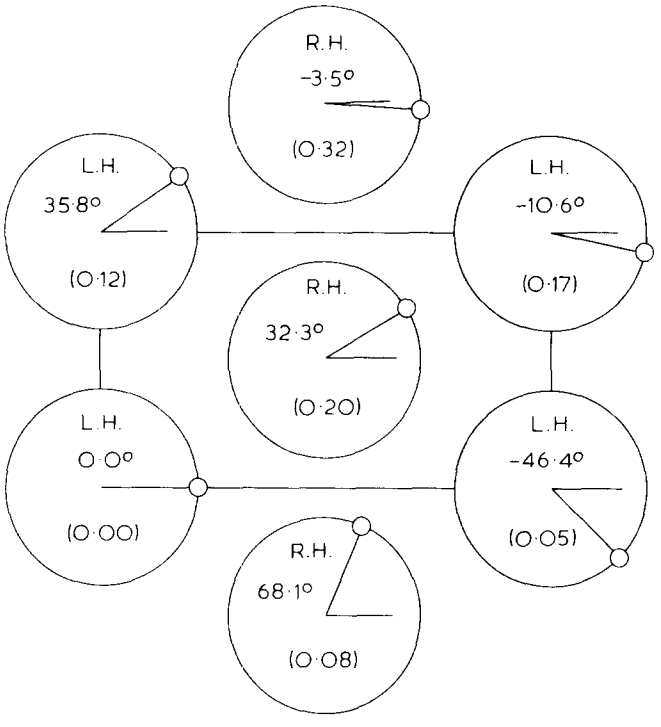

Figure 4 Relative positions of the carbon atom nearest the *x,y*-plane for the crystal structure. Carbon radius not to scale. Numbers in parentheses are translations (in Å units) of the helices along their axes in the direction above the plane

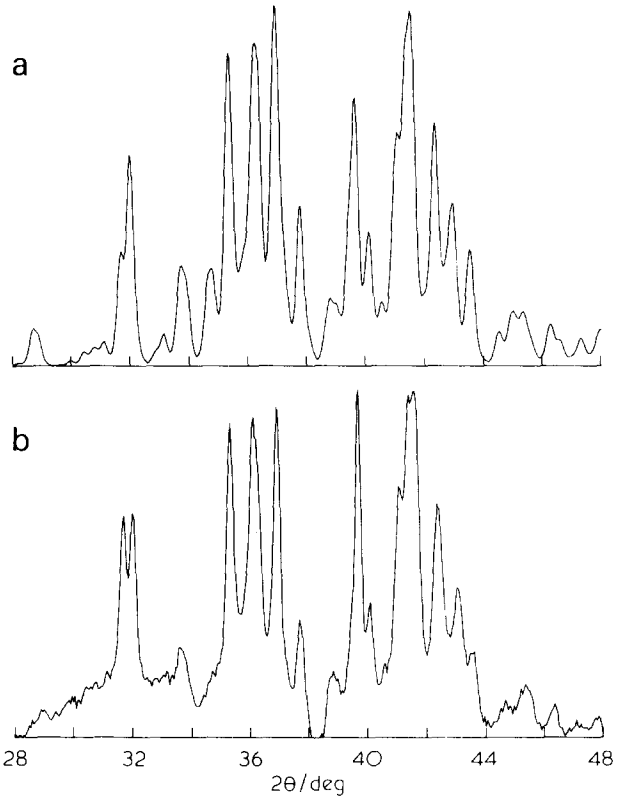

Figure 5 (a) X-ray diffractometer scan calculated for PTFE using the structure with the centre chain rotated and translated as shown in *Figure 4*; (b) the observed diffractometer scan after subtraction of a smooth background

diffraction pattern of *Figure 1*. These cells are listed in *Table 3* and were derived from the 473/219 = 2.1598 helix conformation. All have the same volume and represent packing modes which are nearly identical. All can be represented by *Figure 4* within practical limits of error. Thus, it is not useful to select one of these modes as the 'correct' structure. Furthermore, it is likely that the conformation of the chain will change slightly with temperature giving additional small changes in the packing mode. Since the energy differences among these modes are so small, more than one packing mode may be present in a single sample[16]. Since the diffraction pattern from each mode is essentially the same, the presence or absence of multiple modes cannot be established from our data.

This leads to an interesting finding. Although each of the packing modes of *Table 3* represents essentially the same structure, the conventional triclinic unit cell parameters derived from these modes differ greatly. For example, the parameters derived from packing mode no. 5 (*Table 3*) correspond to the unit cell: $a = 16.27$ nm, $b = 22.48$ nm, $c = 61.49$ nm, $\alpha = 178.6°$, $\beta = 176.6°$, $\gamma = 3.692°$, while that corresponding to cell no. 2 would be: $a = 2.41$ nm, $b = 22.48$ nm, $c = 61.49$ nm, $\alpha = 178.6°$, $\beta = 156.4°$, $\gamma = 23.69°$. Both represent essentially the same structure. Therefore, unique cell parameters cannot be assigned. Also a slight variation in the pitch will change the c-axis from 61.49 nm (473/219 = 2.1598) to 7.02 nm (54/25 = 2.1600) to 123.2 nm (948/439 = 2.1595). Thus, a unique repeat distance cannot be assigned since widely varying c-axis values represent nearly identical conformations. For these reasons, we present for the record our best computational cell, no. 2 of *Table 3*, in terms of lattice parameters r and α so that these values will not be reported as our determination of a crystallographic unit cell:

(I) From electron diffraction(20)

$r_1 = 2.406$ nm, $r_2 = 22.483$ nm, $r_3 = 61.486$ nm
$\alpha_1 = 178.56°$, $\alpha_2 = 156.35°$, $\alpha_3 = 23.69$

(II) From X-ray diffraction (intensity)

$r_1 = 2.407$ nm, $r_2 = 22.483$ nm, $r_3 = 61.486$ nm
$\alpha_1 = 178.56°$, $\alpha_2 = 156.36°$, $\alpha_3 = 23.68°$

For reporting purposes, phase II of polytetrafluoroethylene can be represented by the following parameters: $a'' = 0.9649$ nm, $b'' = 0.5648$ nm, $\gamma'' = 90°$; $c = 0.1300$ nm per CF_2 group; volume = 0.03542 nm^3 per CF_2 group; calculated density = 2344 kg m^{-3}. Repeating motif: two chain stems of opposite hand with a conformation of approximately 2.1598 CF_2 groups per turn of helix of pitch $P = 0.2808$ nm with CF_2 groups at an axial spacing $s = 0.1300$ nm. *Figure 4* gives the rotations of adjacent chains about their axes and translations from a plane normal to the chain direction.

A general procedure is given for finding the best commensurable helix (up to 500 turns) from the layer line spacings.

ACKNOWLEDGEMENT

The authors express their thanks to Dr Edward Prince at NBS for his valuable suggestions and comments.

REFERENCES

1 Bunn, C. W. and Howells, E. R. *Nature (London)* 1954, **174**,549
2 Clark, E. S. and Muus, L. T. *Z. Krist* 1962, **117**, 119
3 Clark, E. S. *Bull. Am. Phys. Soc.* 1973, **18**, 317
4 Clark, E. S., Weeks, J. J. and Eby, R. K. *ACS Symposium Series* 1980, **141**, 183
5 Boerio, F. J. and Koenig, J. L. *J. Chem. Phys.* 1971, **54**, 3667
6 Johnson, K. W. and Rabolt, J. F. *J. Chem. Phys.* 1973, **58**, 4536
7 Chantry, G. W., Fleming, J. W., Nicol, E. A., Willis, H. A., Cudby, M. E. A. and Boerio, F. J. *Polymer* 1974, **15**, 69
8 Kilian, H. G. *Kolloid Z. und Z. für Polymere* 1962, **185**, 13
9 Weeks, J. J., Sanchez, I. C., Eby, R. K. and Poser, C. I. *Polymer* 1980, **21**, 325
10 See e.g. Buerger, M. J. 'X-Ray Crystallography', John Wiley and Sons, Inc., New York, London, Sydney, 1942
11 Santoro, A. and Mighell, A. D. *Acta Cryst.* 1972, **A28**, 284
12 Cochran, W., Crick, F. H. C. and Vand, V. *Acta Cryst.* 1952, **5**, 581
13 Draper, N. R. and Smith, H. 'Applied Regression Analysis', John Wiley and Sons, Inc., New York, London, Sydney, 1966, pp 26–33
14 Malmros, G. and Thomas, J. O. *J. Appl. Cryst.* 1977, **10**, 7
15 Clark, E. S. and Muus, L. T. *Z. Krist.* 1962, **117**, 108
16 Farmer, B. L. and Eby, R. K. *Polymer* 1981, **22**, 1487